Magnetostatic modes and polaritons in antiferromagnetic-non-magnetic superlattices

1992 J. Phys.: Condens. Matter 4 8497

(http://iopscience.iop.org/0953-8984/4/44/011)

J. Phys.: Condens. Matter 4 (1992) 8497–8510. Printed in the UK

Magnetostatic modes and polaritons in antiferromagnetic–non-magnetic superlattices

M C Oliveros†, N S Almeida‡, D R Tilley‡, J Thomas§ and R E Camley§

† Departamento de Fisica Teorica e Experimental/CCE, Universidade Federal do Rio Grande do Norte, 59 072 Natal RN, Brazil

‡ Department of Physics, University of Essex, Colchester CO4 3SQ, Essex, UK

§ Department of Physics, University of Colorado, Colorado Springs, CO 80933-7150, USA

Received 27 July 1992

Abstract. The effective-medium permeability tensor is derived for an antiferromagnet–non-magnet superlattice with uniaxis parallel to the interfaces and an applied magnetic field along the uniaxis. It is used in a calculation of surface-magnetostatic-mode dispersion curves, and it is shown first that the magnetostatic modes are non-reciprocal, $\omega(-q) \neq \omega(q)$, and second that there is no magnetostatic mode for $f_M < 0.5$ where f_M is the volume fraction of the antiferromagnet. Expressions for the dispersion curves of surface polariton modes for a general direction of propagation are derived and illustrated for the Voigt geometry, propagation transverse to the magnetic field. For $f_M > 0.5$ two real and one virtual mode are found, where a 'real' mode is one with a magnetostatic limit. For $f_M < 0.5$ both real modes become virtual. Attenuated total reflection (ATR) curves are calculated; it is seen that they are a sensitive probe of the surface polariton spectrum.

1. Introduction

The electrodynamics of superlattices has been studied at least since the work of Rytov (1955). That paper and much of the subsequent work used a bulk-slab model, in which each layer is treated as being composed of the corresponding bulk material. This model may be conveniently treated within a transfer-matrix formalism (Raj and Tilley 1989), in which the transfer matrix T translates field amplitudes across one period of the superlattice. The transfer matrix is developed using the electromagnetic boundary conditions. For an infinite superlattice, application of Bloch's theorem leads to a dispersion equation for electrodynamic propagation of the form

$$\cos[Q(d_1 + d_2)] = \tfrac{1}{2}\mathrm{Tr}(\mathsf{T}) \tag{1}$$

where Q is the Bloch vector and $d_1 + d_2$ the superlattice period. This equation is exact within the bulk-slab model, and takes into account all multiple reflections at the interfaces.

A significant simplification of (1) can be obtained in some cases. In the far infrared, the radiation wavelength is much greater than the period D, so that in (1) $QD \ll 1$ and in addition usually $q_1 d_1 \ll 1$, $q_2 d_2 \ll 1$, where d_i and q_i are the thicknesses of the two layers and the wavenumbers of the equivalent bulk medium respectively. The trigonometric (or hyperbolic) functions occurring in (1)

0953-8984/92/448497+14$07.50

can therefore be expanded to order Q^2 (Raj and Tilley 1985); the expanded form is identical to the equation for optical propagation in a single uniaxial effective medium with dielectric-tensor components given by

$$\epsilon_{xx} = f_1\epsilon_1 + f_2\epsilon_2 \tag{2}$$

$$\epsilon_{yy}^{-1} = f_1\epsilon_1^{-1} + f_2\epsilon_2^{-1} \tag{3}$$

where the y axis is normal to the interfaces and $f_i = d_i/(d_1 + d_2)$ is the volume fraction of material i. This result can also be derived by a simple field-continuity argument (Agranovich and Kravstov 1985). Far-infrared studies of long-period superlattices, for example, Maslin *et al* (1986), Perkowitz *et al* (1987), have usually described the superlattice part of the sample within the effective-medium description given by (2) and (3). An alternative is to use a standard multilayer optics formalism to calculate reflectivity, for example, with each layer of the superlattice treated separately. Where both methods have been applied to the same data (Jahne *et al* 1991) the parameter values found for the component layers are in agreement.

Since the effective-medium limit of the bulk-slab model proved so useful for semiconductor superlattices it was natural that it should be developed for the magnetic case. This has been done both by expansion (Raj and Tilley 1987) and field-continuity (Almeida and Mills 1988) methods. The general expressions for the effective-medium permeability tensor are quite complicated, largely because the (gyromagnetic) permeability tensor of each component layer contains off-diagonal elements.

While semiconductor superlattices have been studied thoroughly both theoretically and experimentally for excitations in the infrared, the study of magnetic superlattices is not as well developed, particularly on the experimental side. However, ATR (attenuated total reflection) results for magnetic samples may soon be available. Thus in this paper we give a complete description of the bulk and surface electromagnetic modes in a stack of alternating antiferromagnetic and non-magnetic films subjected to a DC magnetic field applied parallel to the easy axis. We use the effective-medium approach to describe the layered system as a homogeneous and anisotropic medium. In order to compare to future experimental work, we also calculate the ATR spectrum for a number of different configurations. In this, we pay particular attention to the application of a magnetic field in the plane of the films as this introduces non-reciprocity in the propagation of the surface modes.

To put this work into perspective, we briefly review some earlier studies. The bulk-slab model (but not using the effective medium) has been used to discuss a number of magnetic superlattices. For example, the well-known result that a surface magnetostatic mode occurs on a ferromagnetic–non-magnetic (M-NM) superlattice only if $f_M > f_{NM}$ was derived in the bulk-slab model (Camley *et al* 1983, Grünberg and Mika 1983) and later confirmed experimentally (Grimsditch *et al* 1983, Kueny *et al* 1984). Here f_M and f_{NM} are the volume fractions of M and NM, so that $f_M + f_{NM} = 1$. Most of this earlier work dealt with ferromagnetic systems with low frequency (5–30 GHz) excitations and with wavevectors of the order of 10^5 cm^{-1}.

In contrast to the studies on ferromagnetic materials, many antiferromagnetic and rare-earth resonance frequencies and ferrimagnetic exchange-resonance frequencies lie in the infrared frequency range of 100 GHz to 10 THz. In this range coupling to electromagnetic radiation is possible with wavenumbers on the order of 3 to 500 cm^{-1}. Thus the programme of far-infrared studies of semiconductor superlattices which is being pursued in several laboratories (Jahne *et al* 1991, Perkowitz *et al* 1987, Samson *et al* 1992, for example) can, in principle, be extended to these magnetic systems.

We earlier carried out (Almeida and Tilley 1990) a study of antiferromagnet–antiferromagnet (AF–AF) and antiferromagnet–non-magnetic (AF–NM) superlattices within the effective-medium description. In this work, no applied static field was included; this led to the considerable simplication that the RF permeability tensor of the antiferromagnet is diagonal, and the effective-medium expression are much simpler than in the general case. Subsequently, FeF_2/CoF_2 superlattices were grown (Ramos *et al* 1990). Since the magnetic ordering direction in these may be normal to the interfaces, the earlier work was extended to this case (Camley *et al* 1992). These studies showed that for the detection of surface polaritons by attenuated total reflection (ATR) a frequency resolution of the order of 0.01 cm^{-1} is required and an angle of incidence of 45° in a Si prism (as distinct from the 20° used for semiconductor studies) is suitable. Thus high-resolution spectroscopy is required; the experiments are technically demanding but not impossible.

As mentioned, in this work we include the effects of a static magnetic field applied parallel to the surface. One of the consequences is that the surface magnetic modes, either magnetostatic or retarded (polariton) can be non-reciprocal, i.e. $\omega(q) \neq \omega(-q)$, where q is the propagation wavevector parallel to the surface. This arises from the absence of time-reversal invariance, manifested by the off-diagonal permeability elements, together with the reduction of spatial symmetry at the surface (Camley 1987). For retarded modes in magnetic systems, non-reciprocity has been observed only somewhat indirectly in reflection experiments (Remer *et al* 1986) and not directly, such as by observation of surface polaritons in ATR. Since experimental work may soon be available, it is timely to extend the results of Almeida and Tilley (1990) to include applied fields, and that is the aim of this paper. The non-reciprocity of the surface modes appear clearly in the ATR spectrum. While the effect of the field is significant, we take external fields small enough so that no spin flop transition takes place.

The remainder of the paper is as follows. The basic effective-medium expressions are given in section 2. The dispersion relation for the surface magnetostatic modes is derived and illustrated in section 3. These modes are equivalent to the Damon–Eshbach (1961) modes for the ferromagnet. The bulk and surface polariton dispersion relations are investigated in section 4. In section 5 we show how these retarded modes can be probed in an ATR experiment. In sections 3 to 5 illustrative numerical results are given for the MnF_2/ZnF_2 superlattice. Conclusions of this work and discussion of possible developments are presented in section 6.

Before concluding this section, we comment on when the bulk-slab model is not appropriate. First, many superlattices, particularly those composed of semiconductors, contain individual layers only a few monolayers thick. The bulk-slab model is inapplicable to these, since a very thin layer cannot simply have the magnetic and dielectric response of a bulk medium. A much more sophisticated analysis is then required; in undoped semiconductors, for example, the contributions of confined optic phonons to the dielectric response of the whole superlattice are included (Samson *et al* 1992). Second, there are a number of cases in which the character of the interface exchange constants or some geometric feature leads to a magnetic ordering which is unique to the superlattice. Two examples are the 'twisted' phase of Fe/Gd (Camley and Tilley 1988) which results from an antiferromagnetic interface interaction between the two ferromagnets, and the period-doubled magnetic structure that can be observed in Gd/Dy (Camley *et al* 1990). Here again, the magnetic structure of the superlattice differs significantly from that of the bulk materials. In such cases,

the permeability for the superlattice can be position-dependent. This is as yet an unsolved problem.

2. Effective-medium theory

We consider a semi-infinite stack of alternating antiferromagnetic and non-magnetic layers with the orientation displayed in figure 1. The coordinate z axis is chosen parallel to the easy axis of the magnetic films and the specimen fills the half space $y \leqslant 0$ with its surface parallel to the x–y plane. It is also considered that the sample is in the presence of a DC magnetic field, applied parallel to the easy axis ($\boldsymbol{H} = H_0\boldsymbol{z}$), which is small compared with the spin flop phase transition field. It is assumed that each individual film is described by the bulk parameters so the non-magnetic layers are described by the dielectric and magnetic permeability tensors $\epsilon_2 = \epsilon_2\mathbf{I}$ and $\mu_2 = \mathbf{I}$ respectively, with $\mathbf{I}$ denoting the identity tensor. The antiferromagnetic layers have their corresponding quantities given by

$$\epsilon = \begin{bmatrix} \epsilon_1 & 0 & 0 \\ 0 & \epsilon_1 & 0 \\ 0 & 0 & \epsilon_3 \end{bmatrix} \tag{4}$$

and

$$\mu = \begin{bmatrix} \mu_1 & i\mu_\perp & 0 \\ -i\mu_\perp & \mu_1 & 0 \\ 0 & 0 & \mu_0 \end{bmatrix}. \tag{5}$$

For a uniaxial Heisenberg antiferromagnet it is known that $\mu_0 = 1$ and the other elements of the tensor are given by Mills and Burstein (1974)

$$\mu_1 = 1 + 4\pi\gamma^2 H_a M_s \left[1/\left(\Omega_r^2 - (\Omega - \gamma H_0)^2\right) + 1/\left(\Omega_r^2 - (\Omega + \gamma H_0)^2\right)\right] \tag{6}$$

$$\mu_\perp = 4\pi\gamma^2 H_a M_s \left[1/\left(\Omega_r^2 - (\Omega - \gamma H_0)^2\right) - 1/\left(\Omega_r^2 - (\Omega + \gamma H_0)^2\right)\right] \tag{7}$$

where γ is the gyromagnetic ratio and Ω_r is the resonance frequency, $\Omega_r^2 = \gamma^2(2H_aH_e + H_a^2)$ with H_a and H_e denoting the anisotropy and exchange fields.

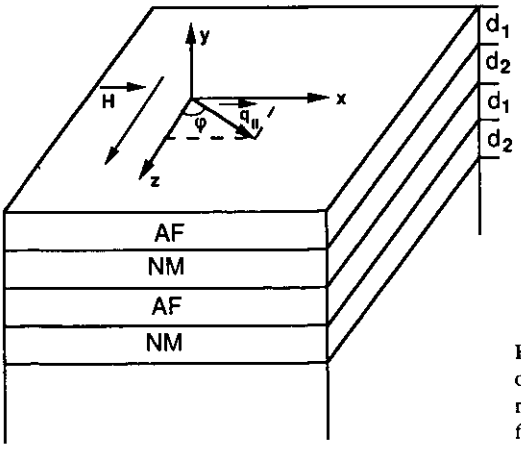

Figure 1. Illustration of superlattice composed of alternating antiferromagnetic and non-magnetic materials. $\boldsymbol{H} = H_0\boldsymbol{z}$ is the external DC magnetic field, d_1 and d_2 are the thicknesses of the layers.

Using the usual method (Raj and Tilley 1987, Almeida and Mills 1988) we find the effective anisotropic tensors which describe the layered system given by

$$\epsilon_{\text{eff}} = \begin{bmatrix} (f_1\epsilon_x + f_2\epsilon_2) & 0 & 0 \\ 0 & [f_1/\epsilon_x + f_2/\epsilon_2] & 0 \\ 0 & 0 & (f_1\epsilon_z + f_2\epsilon_2) \end{bmatrix} = \begin{bmatrix} \epsilon_x & 0 & 0 \\ 0 & \epsilon_y & 0 \\ 0 & 0 & \epsilon_z \end{bmatrix} \tag{8}$$

say, and

$$\mu_{\text{eff}} = \begin{bmatrix} \mu_x & \mathrm{i}\mu_{\text{p}} & 0 \\ -\mathrm{i}\mu_{\text{p}} & \mu_y & 0 \\ 0 & 0 & \mu_0 \end{bmatrix} \tag{9}$$

where

$$\mu_x = [1/(f_1 + f_2\mu_1)]\left[\left(f_1^2 + f_2^2\right)\mu_1 + f_1 f_2\left(1 + \mu_1^2 - \mu_\perp^2\right)\right] \tag{10}$$

$$\mu_y = \mu_1/(f_1 + f_2\mu_1) \tag{11}$$

$$\mu_{\text{p}} = f_1\mu_\perp/(f_1 + f_2\mu_1). \tag{12}$$

Here $f_{\text{i}} = d_{\text{i}}/(d_1 + d_2)$ (i = 1 or 2) with d_1 and d_2 denoting the thickness of the magnetic and non-magnetic layers respectively.

The calculations in this paper are carried out for an MnF_2/ZnF_2 superlattice. The parameters for MnF_2 are $\epsilon_1 = 4$, $\epsilon_3 = 5.5$, $H_{\text{a}} = 7.85$ kG, $H_{\text{e}} = 550$ kG, $M_{\text{s}} = 0.6$ kG. For ZnF_2 we take $\epsilon_2 = 8$. These values give an antiferromagnetic resonance frequency of about 260 GHz.

3. Magnetostatic modes

The knowledge of μ_{eff} allows a complete study of the mixed modes in the superlattice, treated as homogeneous anisotropic material. The dispersion relations for magnetostatic bulk and surface modes are obtained from Maxwell equations

$$\nabla \times \boldsymbol{h} = 0 \tag{13}$$

$$\nabla \cdot (\mu_{\text{eff}} \cdot \boldsymbol{h}) = 0 \tag{14}$$

with $\boldsymbol{h}$ denoting the magnetic field of the excitation. As usual, we use (13) to define this field as the gradient of a scalar magnetic potential $\phi_{\text{m}}(\boldsymbol{h} = -\nabla\phi_{\text{m}})$ and the substitution of this definition in (14) gives the following implicit dispersion relation for the bulk magnetostatic modes

$$\mu_x \cos^2\theta_x + \mu_y \cos^2\theta_y + \mu_0 \cos^2\theta_z = 0 \tag{15}$$

where θ_x, θ_y and θ_z denote the angles between the wavevector of the mode and the x, y and z axis respectively.

For surface modes we have vacuum in the region $y \geqslant 0$ and so we assume solutions for ϕ_{m} in the form

$$\phi_{\text{m}} = \begin{cases} \phi_1 \exp(\mathrm{i}(\boldsymbol{q}_{\|} \cdot \boldsymbol{r}_{\|} - \Omega t) + \alpha_1 y) & \text{if } y \leqslant 0 \\ \phi_2 \exp(\mathrm{i}(\boldsymbol{q}_{\|} \cdot \boldsymbol{r}_{\|} - \Omega t) - \alpha_0 y) & \text{if } y \geqslant 0 \end{cases} \tag{16}$$

where $\boldsymbol{r}_{\|}$, $\boldsymbol{q}_{\|}$ and Ω are the position, wavevector and the frequency of the mode propagating at the surface $y = 0$. Also α_1 and α_2 (both greater than zero) are the decay constants which assure the behaviour expected for a surface mode.

Straightforward algebra gives the following implicit dispersion relation for these modes

$$(1 + \mu_p \sin\varphi)^2 - \mu_y(\mu_x \sin^2\varphi + \mu_0 \cos^2\varphi) = 0 \tag{17}$$

with the subsidiary condition

$$f_1(\mu_\perp/\mu_1)\sin\varphi + 1/\mu_y < 0. \tag{18}$$

In (17) and (18), φ is the angle between the direction of propagation and the z axis, as shown in figure 1. The dispersion relation for the Damon–Eshbach modes is obtained by the solution of (17) provided the subsidiary condition (18) is satisfied.

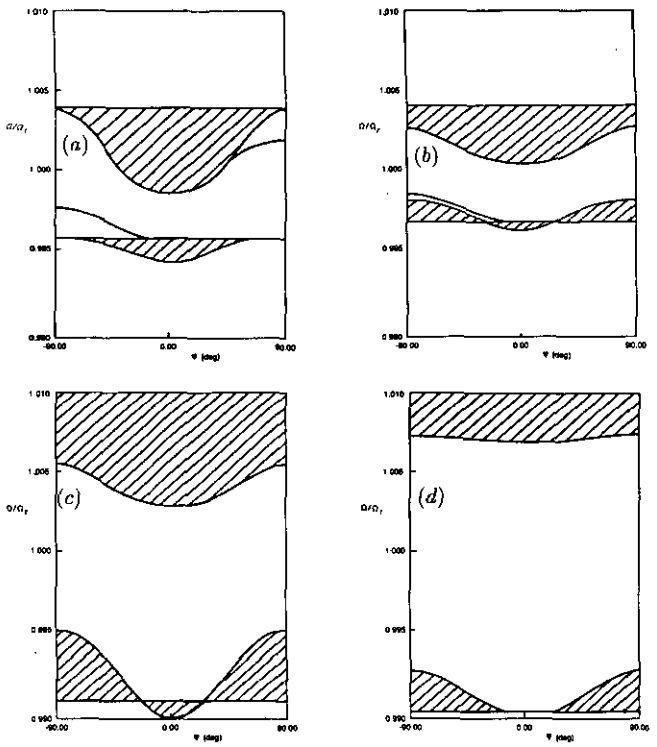

Figure 2. Dispersion relation for magnetostatic modes (*solid curves*) assuming H_0 = 200 G and (*a*) f_1 = 1 (pure AF), (*b*) f_1 = 0.75, (*c*) f_1 = 0.5 and (*d*) f_1 = 0.25. Bulk continua shown shaded.

We shown in figures 2(*a*)–2(*d*) the dispersion relation Ω/Ω_r versus φ for bulk and surface models in an MnF_2/ZnF_2 superlattice obtained from (15) and (17) for different relative thicknesses of the antiferromagnetic component and H_0 = 200 G. In these graphs the shaded areas show the frequency region where there are bulk modes with wavevectors which have their components parallel to the surface in the direction indicated on the horizontal axis and perpendicular component between zero and infinity. The dispersion relations for surface modes are represented by the full lines. The result for f_1 = 1 (pure AF) was obtained by Camley (1980); like the other graphs it shown non-reciprocal propagation, with the lower branch occurring for $\varphi <$ 0 and the upper branch for $\varphi > 0$. Comparing the different graphs in figure 2, one

sees that as f_1 decreases the surface-mode dispersion curves change very little, but the bulk continuum expands towards the surface-mode curves in such a way that the surface modes are completely absorbed within the bulk continua for $f_1 \leqslant 0.5$. It was predicted (Camley *et al* 1983, Grünberg and Mika 1983) and confirmed (Grimsditch *et al* 1983, Kueny *et al* 1984) some time ago that the DE mode would appear on a ferromagnet–non-magnet superlattice only for $f_1 \geqslant 0.5$. The same was found to hold for AF-NM superlattice in the absence of an applied field (Almeida and Tilley 1990), and the present result is a further generalization. Results like those in figure 2 suggest that it should be possible to control the region of propagation of these modes by choosing specific values for the ratio between the thicknesses of the layers.

4. Retarded modes in antiferromagnetic superlattices

Retarded modes are studied in taking Maxwell's equations in complete form, i.e. including retarded terms in the right hand side of (13). After some algebra it is found that the magnetic field of the mode with frequency Ω must obey the following homogeneous wave equation

$$\nabla \times (\epsilon_{\text{eff}}^{-1} \cdot \nabla \times h) - (\omega^2/c^2)\mu_{\text{eff}} \cdot h = 0. \tag{19}$$

For bulk modes we assume the spatial dependence $\exp(iq \cdot r)$ and the dispersion relation is obtained by setting the determinant of the coefficient matrix equal to zero. Since for each value of 2D wavevector $q_{\parallel}$ parallel to the surface we can have any value from zero to infinity for the perpendicular component q_y we find in the Ω–$q_{\parallel}$ plane not a single curve but a frequency region where these modes exist.

Surface polaritons are localized at the surface and have their magnetic field given by

$$h = h_0 \exp(iq_{\parallel} \cdot r - \alpha_0 y) \qquad (y \geqslant 0) \tag{20}$$

$$h = h_1 \exp(iq_{\parallel} \cdot r + \alpha_1 y) \qquad (y \leqslant 0) \tag{21}$$

where α_1 and α_0 are decay factors that are real and greater than zero. Using the effective dielectric (ϵ_{eff}) and magnetic permeability (μ_{eff}) tensors defined earlier, we find that the magnetic field h obeys the following matrix equation

$$\mathbf{A}h = 0 \tag{22}$$

where

$$A_{ii} = -\frac{1}{\epsilon_{kk}}\frac{\partial}{\partial x_j^2} - \frac{1}{\epsilon_{jj}}\frac{\partial}{\partial x_k^2} - \frac{\Omega^2}{c^2}\mu_{ii} \tag{23}$$

$$A_{ij} = \frac{1}{\epsilon_{kk}}\frac{\partial^2}{\partial x_i \partial x_j} - \frac{\Omega^2}{c^2}\mu_{ij}. \tag{24}$$

In the equations above, i, j, k assume values 1, 2, 3 in cyclic order. The condition for a non-trivial solution of (22) and the boundary conditions for the electromagnetic fields at the surface of the specimen given for the surface mode propagating in a φ direction (φ is the angle between $q_{\parallel}$ and the z axis) the following two equations for α_1

$$(\mu_y \sin\varphi)\alpha_1^2 + \left[\alpha_0\left(\epsilon_x\mu_y + \mu_x\mu_y - \mu_p^2\right)\sin\varphi - \mu_p q_{\parallel}\right]\alpha_1$$

$$-\epsilon_x(\omega^2/c^2 - q_\parallel^2\sin^2\varphi)\left(\mu_x\mu_y - \mu_p^2\right)\sin\varphi$$
$$+ q_\parallel^2(\mu_x + \epsilon_x\mu_y - 1)\sin\varphi\cos^2\varphi$$
$$-\alpha_0 q_\parallel\mu_p\left(\cos^2\varphi + \epsilon_x\sin^2\varphi\right) = 0 \tag{25}$$

and

$$\left(\frac{\epsilon_z^2}{\epsilon_x}\mu_y\frac{\Omega^2}{c^2}\right)\alpha_1^4 - \left\{\left[q_\parallel^2\left(\frac{\epsilon_z}{\epsilon_x}\cos^2\varphi + \sin^2\varphi\right) - \epsilon_z\mu_y\frac{\Omega^2}{c^2}\right]\right.$$
$$\times\left[-\frac{\epsilon_x}{\epsilon_y}q_\parallel^2\left(\frac{\epsilon_z}{\epsilon_x}\cos^2\varphi + \sin^2\varphi\right) + \epsilon_z\left(\frac{\epsilon_z}{\epsilon_x}\mu_x + 1\right)\frac{\Omega^2}{c^2}\right]$$
$$-\epsilon_z\frac{\Omega^2}{c^2}q_\parallel^2\left[\sin^2\varphi + \left(\frac{\epsilon_z}{\epsilon_x}\right)^2\mu_x\cos^2\varphi\right]$$
$$\left.+\frac{\epsilon_z}{\epsilon_y}q_\parallel^4\left(\frac{\epsilon_z}{\epsilon_x}\cos^2\varphi + \sin^2\varphi\right)^2 - \frac{\Omega^4}{c^4}\frac{\epsilon_z^3}{\epsilon_x}\mu_p^2\right\}\alpha_1^2$$
$$-\left[q_\parallel^2\left(\frac{\epsilon_z}{\epsilon_x}\cos^2\varphi + \sin^2\varphi\right) - \epsilon_z\mu_y\frac{\Omega^2}{c^2}\right]$$
$$\times\left[\epsilon_z^2\mu_x\frac{\Omega^4}{c^4} - \frac{\epsilon_z^2}{\epsilon_y}\frac{\Omega^2}{c^2}q_\parallel^2\left(\cos^2\varphi + \mu_x\sin^2\varphi\right)\right]$$
$$-\epsilon_z^2\mu_p^2\frac{\Omega^4}{c^4}\left(\frac{\epsilon_z}{\epsilon_y}q_\parallel^2\sin^2\varphi - \epsilon_z\frac{\Omega^2}{c^2}\right) = 0. \tag{26}$$

Since α_1 is a function of ω and $q_\parallel$, the values of this decay factor for which both equations above are satisfied and also are greater than zero give us the dispersion relation required. The direction of propagation parallel to the x axis (Voigt geometry) has a particularly simple dispersion relation since $\varphi = \pi/2$ and (25) and (26) become

$$\alpha_1^2 = \frac{\mu_x}{\mu_y}\left[q_\parallel^2 - \epsilon_z\mu_y\frac{\omega^2}{c^2}\right] + \epsilon_z\frac{\omega^2}{c^2}\frac{\mu_p^2}{\mu_y} \tag{27}$$

$$\alpha_1 = -(1/\mu_y)\left[\alpha_0\left(\mu_x\mu_y - \mu_p^2\right) - q_\parallel\mu_p\right] \tag{28}$$

resulting in the following relation

$$\left(q_\parallel^2 - \Omega^2/c^2\right)\left(\mu_x\mu_y - \mu_p^2\right) - 2q_\parallel\mu_p\left(q_\parallel^2 - \Omega^2/c^2\right)^{1/2} - \left(q_\parallel^2 - \epsilon_z\mu_y\Omega^2/c^2\right) = 0. \tag{29}$$

The non-reciprocity is apparent here in the appearance of a term linear in $q_\parallel$. The values of Ω and $q_\parallel$ that satisfy (29) and also give for α_1 (from (28)) a value greater than zero are the required solution.

Examples of dispersion curves calculated for the MnF_2/ZnF_2 superlattice are shown in figure 3. Attention is restricted to the Voigt geometry, $\varphi = \pi/2$. It is seen that even with a fairly modest applied field the non-reciprocity is striking. Figure 3(*a*) is the result for pure MnF_2 ($f_A = 1$) and is the same as has been shown previously (Camley 1987). The upper bulk continuum predicted for $H_0 = 0$ splits into two, with a new surface mode appearing on the $-k$ side in the gap between the

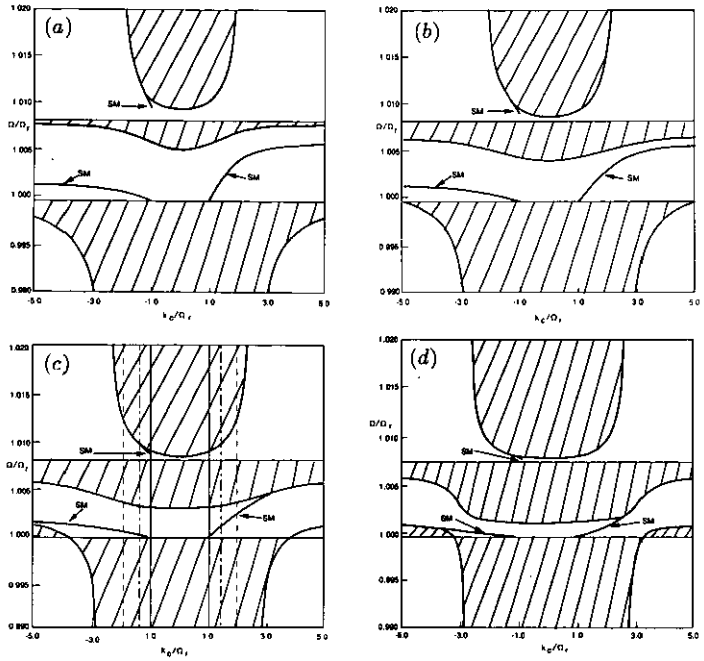

Figure 3. Dispersion relation for retarded modes (surface polaritons) in Voigt geometry assuming $H_0 = 200$ G and (*a*) $f_1 = 1$ (pure AF), (*b*) $f_1 = 0.75$, (*c*) $f_1 = 0.5$ and (*d*) $f_1 = 0.25$. Bulk continua shown shaded.

two. This mode starts at the low-frequency end on the vacuum light line (essentially the vertical line $ck/\Omega_r = -1$ on the scale used) and terminates at a finite value of k in the uppermost bulk continuum. Thus it has no magnetostatic limit and may be called a virtual mode in the usual terminology. The two lower surface modes, which are already present for $H_0 = 0$, now exhibit marked non-reciprocity. Both have magnetostatic limits, i.e. they are real modes for $f_A = 1$ and the limiting frequencies agree with the corresponding points on figure 2 ($\varphi = \pm 90°$).

Figures 3(*b*) to 3(*d*) show the corresponding curves for progressively decreasing values of f_A. Broadly speaking, the bulk continuum regions expand while the surface-mode curves alter only slightly. The lower surface modes change over from real to virtual at $f_A = 0.5$. Like the corresponding result in the absence of an applied field (Almeida and Tilley 1991) this is a generalization of the result of section 3 that there is no magnetostatic mode for $f_A < 0.5$.

5. Attenuated total reflection

We have shown in figure 3 examples of the dispersion relation for surface polaritons. As commented in section 1, ATR spectroscopy should prove effective in investigating these modes, as it has been for the corresponding modes in layered semiconductor structure (El Gohary *et al* 1989, Haraguchi *et al* 1990, Dumelow *et al* 1991, for example). In the ATR method, shown schematically in figure 4, light is incident at an angle θ_i in a prism of dielectric constant ϵ_s; θ_i is chosen greater than $\theta_c = \sin^{-1} \epsilon_s^{-1/2}$, the critical angle for total internal reflection at the prism–vacuum interface. Simple

kinematic analysis (Cottam and Tilley 1989) shows that the in-plane wavevector component is

$$q_{\parallel} = \epsilon_s^{1/2}(\omega/c)\sin\theta_i \tag{30}$$

and that this applies to the electromagnetic excitations in all the layers. Typically in far-infrared experiments θ_i is fixed and the frequency ω is scanned. Equation (30) then shows that the experimental scan is along a straight line in the $(q_{\parallel}\omega)$ plane. On the scale of figure 3, such scan lines are essentially vertical, and examples for $\theta_i = \pm 25°$ and $\pm 35°$ are shown in figure 3(*c*). The expected spectra may be divided into three types of region. Where the scan line falls within a bulk continuum, coupling across the gap to the bulk modes occurs and the reflectivity R is below unity but generally without sharp features. Outside the bulk continua but away from the immediate vicinity of surface-mode dispersion curves the reststrahl-like property $R = 1$ is expected; in practice, damping within the sample reduces R slightly below 1. At a crossing with a surface-mode dispersion curve R dips sharply below 1 due to the coupling which the technique is designed to achieve. The width of the dip is governed by damping. The damping parameter Γ used here is 150 G. The depth depends on the value of the coupling gap d; for optimal d theoretical curves, but not usually experimental curves, may dip to $R = 0$. The optimal value of d depends on the exponential decay lengths of the evanescent field below the prism and the polariton field above the sample surface. The former increases with the free-space wavelength of the radiation and decreases as θ increases away from θ_c, the critical angle for total internal reflection; the optimal value of d therefore also shows these trends.

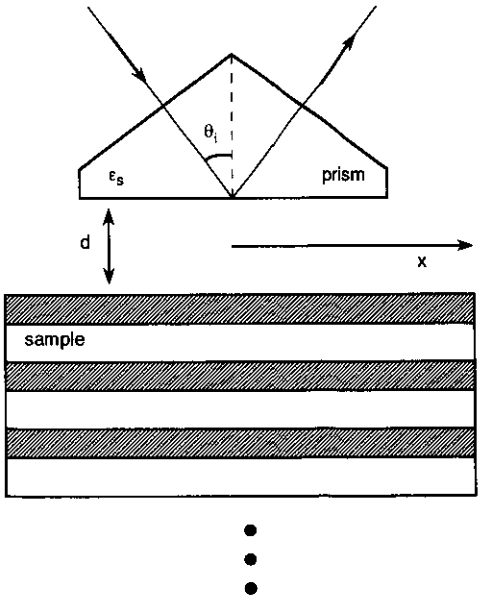

Figure 4. Illustration of the geometry used to obtain the ATR spectrum.

These general features are seen in many experimental ATR spectra, for example, those measured in the far infrared on semiconductor superlattices (Dumelow *et al* 1993).

An explicit formula for the ATR reflectivity in the case when the sample is described by the effective-medium permeability of (9) has been given previously (Almeida and Tilley 1991). ATR spectra calculated from it for the sample of figure 3(*c*) ($f_A = 0.5$) are shown in figure 5. Because of the very fine frequency scale required to show the features of interest, curves for the lower and upper surface-mode windows are shown separately.

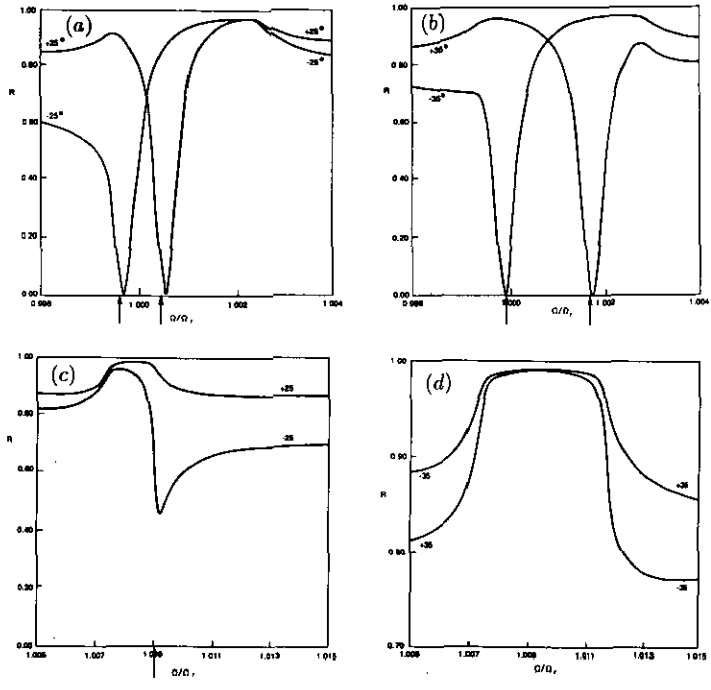

Figure 5. ATR spectrum as a function of frequency calculated using the geometry illustrated in figure 4. Here $f_1 = f_2 = 0.5$, $d = 0.017$ cm, $\epsilon_{prism} = 11.6$ $H = 0.2$ kG. (*a*) $\theta_i = \pm 25°$ (dash-dot lines in figure 3(*c*)), lower window; (*b*) $\theta_i = \pm 35°$ (dashed lines in figure 3(*c*)), lower window; (*c*) $\theta_i = \pm 25°$, upper window; (*d*) $\theta_i = \pm 35°$, upper window. Intersections of scan lines with surface-polariton dispersion curves in figure 3(*c*) are marked with arrows.

Figure 5(*a*) shows the ATR curves for $\theta = \pm 25°$ in the lower window; the non-reciprocity is quite evident, as it is in all subsequent curves, and should be resolvable by a suitable instrument. Both curves start at the low-frequency end with $R < 1$ since the scan line in figure 3(*c*) is then in a bulk continuum. As the frequency increases the scan line enters a reststrahl region with $R \approx 1$; within this region the surface-mode dip is seen. In fact for $\theta_i = -25°$ the surface mode is sufficiently near to the top of the bulk continuum that the onset of the reststrahl region is not seen. At higher frequencies the scan line again enters a bulk continuum with $R < 1$. The curves are drawn for a numerically selected 'optimal d', the criterion being to choose the largest d value for which $R \approx 0$ is attained at the bottom of the dip. In fact the d value for $\theta_i = -25°$ is different from that for $\theta_i = +25°$, presumably because the surface-polariton decay length is different in the two cases. In practice, the magnetic field direction would be reversed to go from one scan to the other, presumably without change of gap setting, but since a sharp ATR dip is found for a

wide range of d-values it is unlikely that there would be any need to reset d. The surface-mode dip is expected to occur at the frequency at which the scan line in figure 3(c) crosses the dispersion curve. On figure 5(a) and the later figures these crossing points are denoted by arrows on the frequency axis; they are seen to coincide quite closely with the dip frequencies.

The corresponding lower-window curves for $\theta_i = \pm 35°$ are shown in figure 5(b); the same general comments apply as for figure 5(a). The gap values are smaller than in figure 5(a) since the evanescent-mode decay length is shorter for the larger angle.

Figure 3(c) shows that the upper $-k$ surface-mode branch intersects the $-25°$ scan but not the $-35°$ scan. The calculated ATR curves for both positive and negative angles of incidence in the upper surface-mode window are shown in figures 5(c) and 5(d). Figure 5(c) for $\theta_i = \pm 25°$ shows the expected and striking non-reciprocity i.e. the surface-mode dip is seen for $-25°$ but not for $+25°$. The dip does not drop to $R = 0$: the curve was calculated for the same value of d as was used for figure 5(a) (as would be the case in an experimental run) and d is not therefore optimized for this branch. Nevertheless, the feature is quite prominent. Otherwise the $+25°$ curve, and the $-25°$ curve outside the surface dip, show the sequence bulk continuum ($R < 1$)–reststrahl ($R \approx 1$)–bulk continuum ($R < 1$) that is to be expected from the scan line in figure 3(c). In contrast to figure 5(c), figure 5(d) shows no surface-mode dip for the $-35°$ scan, and both $\pm 35°$ curves follow the simple sequence bulk continuum–reststrahl–bulk continuum seen in figure 3(c).

The ATR reflectivity as a function of frequency gives very complete information on the surface polariton modes. A typical method of making such a measurement is to use a broad-band source of electromagnetic radiation and pick out the response at the individual frequencies using interferometry. However, due to the narrow frequency range of the surface polaritons, such a measurement is challenging because it requires excellent frequency resolution. We therefore explore two other possible measurement methods. In both cases we imagine illuminating the sample with a single well-defined frequency as is found in a laser. This eliminates the problem of obtaining good frequency resolution.

In the first case we assume the frequency of the external radiation matches that of a surface polariton and arrange to have the parallel wavevector match as well by changing the angle of incidence. The theoretical results for such a measurement are presented in figure 6 where we plot ATR reflectivity as a function of incident angle. This corresponds to scanning across figure 3 at a frequency $\Omega/\Omega_T = 1.002$. In figure 3 we see that at this frequency a surface modes exists only for positive k. This non-reciprocity of the surface polariton modes is clearly demonstrated in the existence of a deep dip for positive θ and the lack of a corresponding dip for negative θ.

The second method is probably more convenient experimentally. Here the incident angle is fixed and the external field is varied. The external field can be used to shift the surface and bulk polaritons up or down in frequency so as to match the frequency of the polaritons to that of the incident radiation. The theoretical results for such an experiment are given in figure 7. Here the non-reciprocity is evident in that positive and negative H give very different results. From figure 7 we see that the shift in the position of the dip between positive H and negative H is about 200 gauss. Such a difference should be easily measurable.

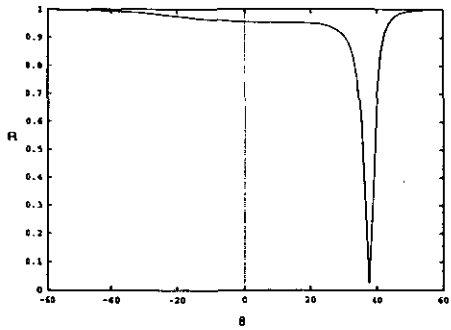

Figure 6. ATR reflectivity as a function of incident angle. The parameters for this calculation are the same as in figure 5 except that the gap is 0.019 cm, $\Omega/\Omega_T = 1.002$ and $\Gamma = 20$ gauss.

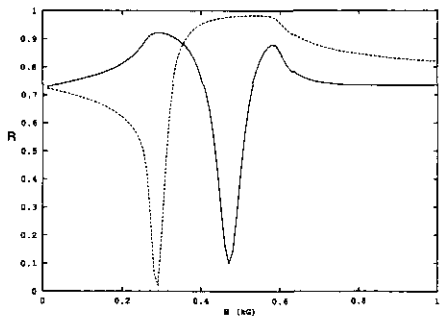

Figure 7. The ATR reflectivity as a function of applied field. Continuous curve $+H$, dashed curve $-H$. The parameters for this calculation are those in figure 6 except that $\Omega/\Omega_T = 0.999$ and $\theta_i = 25°$.

6. Conclusions

The present paper has continued the theoretical study of antiferromagnet-based superlattices by including the effects of an applied static field. This is important not only because it is likely that experimental work will include magnetic field effects, but also because the inclusion of the field means that the RF permeability tensor of the antiferromagnet takes the gyromagnetic form of (5) rather than the simpler diagonal form found without applied field. In consequence, and as seen in figures 2 and 3, non-reciprocal propagation is found, as is very characteristic of magnetic systems. It is striking that the pronounced anisotropy evident in figures 2 and 3 is induced by the modest field value of 200 G, although as seen from (6) and (7) this is essentially scaled by the antiferromagnetic resonance frequency, which is rather low in MnF_2. As in reflectivity (Remer *et al* 1986), the experimental indication of non-reciprocity is that the main ATR dip would be seen at different frequency in a reversed magnetic field.

We have concentrated on surface modes and the related ATR spectra. It is worth commenting, however, that oblique-incidence reflectivity is also a technique with a considerable potential. For semiconductor superlattices, it has been found that oblique-incidence reflectivity spectra yield detailed information on the bulk polariton modes which is very valuable in characterization (Lou *et al* 1988, Dumelow and Tilley 1992). In fact, as pointed out already, the only direct evidence for non-reciprocal propagation on the surface of an antiferromagnetic was obtained by oblique-incidence reflectivity (Remer *et al* 1986).

Here, as in Almeida and Tilley (1990), it has been assumed that the AF uniaxis as well as the applied field lie parallel to the superlattice planes. While such an arrangement is quite possible, it seems likely that in AF–AF superlattices so far reported (Ramos *et al* 1990), the uniaxis lies in the growth direction. The surface polariton spectra and ATR spectra in the absence of a magnetic field for this geometry have been reported elsewhere (Camley *et al* 1992); clearly a useful generalization would be to include an applied field for this geometry.

As mentioned in section 1, a strong enough applied field induces a spin-flop transition, but we have considered only fields sufficiently weak that this does not

occur. In fact the phase diagram (in $T-H-f_1$ space) even for AF/NM superlattice has not been studied in detail; both this and the magnetostatic and polariton modes of the various phases that may occur represent a substantial field of study.

Acknowledgments

MCO and NSA thank the Brazilian agency CNPq for partial financial support. REC and DRT acknowledge support from SERC and NATO. The work of REC was also supported by the US Army Research Office under Grant *DAAL0391-G-0229*. The work of NSA was also supported by the Royal Society.

References

Agranovich V M and Kravstov V E 1985 *Solid State Commun.* **55** 85
Almeida N S and Mills D L 1988 *Phys. Rev.* B **38** 6698
Almeida N S and Tilley D R 1990 *Solid State Commun.* **73** 23
Camley R E 1980 *Phys. Rev. Lett.* **45** 283
—— 1987 *Surf. Sci. Rep.* **7** 103
Camley R E, Cottam M G and Tilley D R 1992 *Solid State Commun.* **81** 571
Camley R E, Kwo J, Hong M and Chien C L 1990 *Phys. Rev. Lett.* **64** 2703
Camley R E, Rahman T S and Mills D L 1983 *Phys. Rev.* B **27** 261
Camley R E and Tilley D R 1988 *Phys. Rev.* B **37** 3413
Cottam M G and Tilley D R 1989 *Introduction to Surface and Superlattice Excitations* (Cambridge: *Cambridge University* Press)
Damon R W and Eshbach J R 1961 *J. Phys. Chem. Solids* **19** 308
Dumelow T, Parker T J, Smith S R P and Tilley D R 1993 *Surf. Sci. Rep.* to appear
Dumelow T, Parker T J, Tilley D R, Beall R B and Harris J J 1991 *Solid State Commun.* **77** 235
Dumelow T and Tilley D R 1992 *Excitations in Superlattices and Multi-Quantum Wells (Springer Series in Physics)* ed M G Cottam and M Singh (Berlin: Springer) at press
El Gohary A R, Parker T J, Raj N, Tilley D R, Dobson P J, Hilton D and Foxon C T B 1989 *Semicond. Sci. Technol.* **4** 388
Grimsditch M, Khan M R, Kueny A and Schuller I K 1983 *Phys. Rev.* B **51** 498
Grünberg P and Mika K *1983 Phys. Rev.* B **27** *2955*
Haraguchi M, Fukui M and Muto S 1990 *Phys. Rev.* B **41** 1254
Jahne E, Roselar A and Ploog K 1991 *Superlatt. Microstruct.* **9** 219
Kueny A, Khan M R, Schuller I K and Grimsditch M 1984 *Phys. Rev.* B **29** 2879
Lou B, Sudharsanan R and Perkowitz S 1988 *Phys. Rev.* B **38** 2212
Maslin K A, Parker T J, Raj N, Tilley D R, Dobson P J, Hilton D and Foxon C T B 1986 *Solid State Commun.* **60** 461
Mills D L and Burstein E 1974 *Rep. Prog. Phys.* **37** 817
Perkowitz S, Sudharsanan R, Harris K A, Cook Jr J W, Schetzina J F and Schulman J N 1987 *Phys. Rev.* B **36** 9290
Raj N and Tilley D R 1985 *Solid State Commun.* **55** 373
—— 1987 *Phys. Rev.* B **36** 7003
—— 1989 The electrodynamics of superlattices *The Dielectric Function of Condensed Systems* ed L V Keldysh, D A Kirzhnitz and A A Maradudin (Amsterdam: Elsevier) ch 7
Ramos C A, Lederman D, King A R and Jaccarino V 1990 *Phys. Rev. Lett.* **65** 2913
Remer L, Luthi B, Sauer H, Geick R and Camley R E 1986 *Phys. Rev. Lett.* **56** 2752
Rytov S M 1955 *Zh. Eksp. Teor. Fiz.* **29** 605 (Engl. Transl. *Sov. Phys. JETP* **2** 466)
Samson B, Dumelow T, Hamilton A A, Parker T J, Smith S R P, Tilley D R, Foxon C T B, Hilton D and Moore K J 1992 *Phys. Rev.* B **46** 2375